applied optics

Fast and accurate focusing analysis of large photon sieve using pinhole ring diffraction model

Tao Liu, Xin Zhang,* Lingjie Wang, Yanxiong Wu, Jizhen Zhang, and Hemeng Qu

Key Laboratory of Optical System Advanced Manufacturing Technology, Changchun Institute of Optics and Fine Mechanics and Physics, Chinese Academy of Sciences, Changchun 130033, China
**Corresponding author: xinliutao@aliyun.com*

Received 5 February 2015; revised 24 April 2015; accepted 4 May 2015; posted 4 May 2015 (Doc. ID 233834); published 4 June 2015

In this paper, we developed a pinhole ring diffraction model for the focusing analysis of a large photon sieve. Instead of analyzing individual pinholes, we discuss the focusing of all of the pinholes in a single ring. An explicit equation for the diffracted field of individual pinhole ring has been proposed. We investigated the validity range of this generalized model and analytically describe the sufficient conditions for the validity of this pinhole ring diffraction model. A practical example and investigation reveals the high accuracy of the pinhole ring diffraction model. This simulation method could be used for fast and accurate focusing analysis of a large photon sieve.

OCIS codes: (050.0050) Diffraction and gratings; (050.1940) Diffraction; (050.1965) Diffractive lenses; (110.0110) Imaging systems; (350.1260) Astronomical optics.

http://dx.doi.org/10.1364/AO.54.005327

1. INTRODUCTION

In 2001, Kipp *et al.* proposed [1] a diffractive focusing element called a photon sieve (PS), which consists of a great number of pinholes distributed over the Fresnel zones. To analyze its focusing property, the paraxial and the nonparaxial far-field model for individual pinholes were proposed by Cao and co-workers [2,3] using the Rayleigh–Sommerfeld diffraction integral. Since then, a lot of work has been done concerning the sidelobe suppression, multiwavelength, or broadband imaging and resolution increase [4–7]. PS has important applications in physical and life sciences, such as in high-resolution microscopy, spectroscopy, X-ray, or EUV lithography. Photon sieve also is one of the appealing solutions for next generation ultra-large (> 20 m) space telescope primaries [8]. Deployable membrane PSs are lightweight and compact in size. Furthermore, apodization, which is the modification of the number of holes per zone, can be incorporated into a PS to modify the resolution and contrast. However, a large PS would consist of an extremely large number of circular pinholes. In Ref. [9], Andersen gave an approximation for the number of holes of a PS:

$$\text{Number} \sim \frac{0.45(D/2)^2}{(f\lambda)^2}, \tag{1}$$

where D, f, and λ are the diameter, focal length, and design wavelength of the PS. Thus, there are millions or even billions of pinholes for a large PS with a big diameter or high numerical aperture (NA). This would greatly increase the difficulty and time for the analysis and optimization of PS.

Instead of evaluating the performance of individual pinholes, we present a fast, accurate analytical pinhole ring diffraction model for the focusing and imaging of the PS within the framework of scalar field. A PS is essentially a Fresnel zone plate in which isolated circular holes are used instead of the rings. The pinholes in each ring usually have the same size and are distributed uniformly in angle about the ring zone. In Section 2, we proved that all of the pinholes in a ring zone could be treated as a single unity when investigating the diffracted field of the small focal region. We give the explicit equation for the diffracted field of an individual pinhole ring. In Section 3, we discussed the validity range of the pinhole ring diffraction model. And one prototype photon sieve was designed to validate this pinhole ring diffraction model. Section 4 concludes our discussion. We believe this simple, yet accurate, analytical model could be used to compute the diffracted fields of individual pinhole rings. In terms of the linear superposition principle, these diffracted fields could be further summed up to quickly analyze the focusing property of big photon sieve.

2. DIFFRACTION MODEL OF PINHOLE RING

As shown in Fig. 1, the photon sieve discussed here is located in the x–y plane and the image plane in the X–Y plane. The PS is

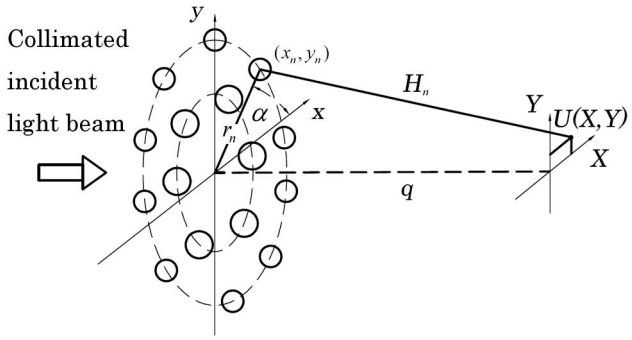

Fig. 1. Schematic view of a general photon sieve with collimated incident light beam.

perpendicularly illuminated by a collimated incident light beam with unit amplitude. We investigated the performance of the mth pinhole ring, which is composed of N_m circular pinholes. Those pinholes have the same size and are distributed uniformly in angle in the ring zone. We denoted the coordinates of the center of the nth circular pinhole in the ring by (x_n, y_n) and the coordinates of the diffracted field by (X, Y). Obviously, the distance from the center of the nth pinhole to the diffracted field is $H_n = [q^2 + (X - x_n)^2 + (Y - y_n)^2]^{1/2}$, where q is the distance from the photon sieve plane to the image plane. In Ref. [3], Cao and Jahns have presented the nonparaxial far-field model to describe the diffracted fields for the individual circular pinholes whose Fresnel numbers $N_f = \pi a_n^2/(\lambda q)$ are smaller than 0.05 and a_n is the radius of the nth circular pinhole. It could be used to analyze the focusing of the pinholes in big or high-NA photon sieves. It should be emphasized that Cao's definition of a nonparaxial case refers to the relatively big off-axis distance between the axis of individual pinholes and the focal region at the image plane. For the imaging of PS, the focal region is quite near the focal point ($X = 0$, $Y = 0$). In other words, the focal region is the nonparaxial area for individual pinholes, but also the paraxial area for the whole PS. Readers should remember these definitions.

We started from Eq. (12) of Ref. [3], which is the nonparaxial far-field distribution of the nth pinhole:

$$U_n(X, Y) = \frac{kA_n a_n^2 q}{H_n^2} \exp[jk(L_n + H_n)] \times Jinc\left(\frac{ka_n}{H_n}\rho\right), \quad (2)$$

where $Jinc(\cdot) = J_1(\cdot)/(\cdot)$, j is the imaginary unit, $k = 2\pi/\lambda$ is the wave number, A_n is the field value of the incident wave at the nth circular pinhole, L_n is the eikonal value at (x_n, y_n), and $\rho = [(X - x_n - g_n H_n)^2 + (Y - y_n - h_n H_n)^2]^{1/2}$, where $g_n = (\partial L/\partial x)|_{x_n, y_n}$ and $h_n = (\partial L/\partial y)|_{x_n, y_n}$. Equation (2) was developed in Ref. [3] to describe the diffracted field distributions for individual pinholes within the framework of scalar field diffraction. The above expressions and definitions can be found in Ref. [3], and are quoted here for our further analysis. It is worth mentioning that Eq. (2) is valid for pinholes whose Fresnel number N_f is smaller than 0.05 and we substituted the expression H in Eq. (12) of Ref. [3] with H_n for our discussion. Also note that the PS is perpendicularly illuminated by a plane wave in our discussion; thus, $L_n = g_n = h_n = 0$ and A_n can be treated as a constant $A_n = 1.0$ here. Besides, it is more convenient to discuss the influence of an individual pinhole ring under a polar coordinate system. By employing the polar coordinate variables R, ϕ, and α through the transforms $R^2 = X^2 + Y^2$, $r_n^2 = x_n^2 + y_n^2$, $X = R\cos\phi$, $Y = R\sin\phi$, $x_n = r_n\cos\alpha$, and $y_n = r_n\sin\alpha$, and substituting all of these relations into Eq. (2), we could obtain

$$U_n(R, \phi) = \frac{kA_n a_n^2 q}{H_n^2} \exp(jkH_n) \times Jinc\left\{\frac{ka_n}{H_n}\left[(R\cos\phi - r_n\cos\alpha)^2 + (R\sin\phi - r_n\sin\alpha)^2\right]^{1/2}\right\}. \quad (3)$$

According to the linear superposition principle, the total diffracted field $U_m(X, Y)$ at the image plane for those pinholes that are centered on the mth ring can be calculated by the summation of those individual diffracted fields. Then one can obtain

$$U_m(R, \phi) = \sum_{n=1}^{N_m} \frac{kA_n a_n^2 q}{H_n^2} \exp(jkH_n) \times Jinc\left\{\frac{ka_n}{H_n}\left[(R\cos\phi - r_n\cos\alpha)^2 + (R\sin\phi - r_n\sin\alpha)^2\right]^{1/2}\right\}. \quad (4)$$

In the common case, the area of interest at the image plane is actually the focal area where the radial coordinate R is very small. That is because the focal spot is usually quite small for a photon sieve. When $R \ll r_n$, we could use the following approximation:

$$[(R\cos\phi - r_n\cos\alpha)^2 + (R\sin\phi - r_n\sin\alpha)^2]^{1/2} \approx r_n. \quad (5)$$

Then, let us focus on the value of H_n, which could be expressed as

$$H_n = [q^2 + R^2 + r_n^2 - 2Rr_n\cos(\phi + \alpha)]^{1/2}, \quad (6)$$

in polar coordinate. In terms of binomial expansion, H_n could be rewritten as

$$H_n \approx H_0 - \frac{Rr_n\cos(\phi + \alpha)}{H_0}, \quad (7)$$

where $H_0 = (q^2 + R^2 + r_n^2)^{1/2}$. Note the higher terms of the expansion are ignored in Eq. (7). We used the approximation Eq. (7) for the H_n in the exponent of Eq. (4). For the two H_n in the denominators of Eq. (4), the first term on the right-hand side of Eq. (7) is already good enough due to the relatively small value of R. The accuracy of the above approximations from Eq. (5) to Eq. (7) relies on the condition of $R \ll r_n$. As we shall show in the second paragraph in Section 3, the approximations are accurate enough when $R/r_n \le 0.05$. Substituting these approximations into Eq. (4), one can get

$$U_m(R, \phi) = \frac{kA_n a_n^2 q}{H_0^2} Jinc\left(\frac{ka_n}{H_0}r_n\right) \exp(jkH_0) \times \sum_{n=1}^{N_m} \exp\left[-jk\frac{Rr_n\cos(\phi + \alpha)}{H_0}\right]. \quad (8)$$

Since the system discussed here could be treated as circularly symmetric about R, the function $U_m(R,\phi)$ must be independent of the angle ϕ. In this case, we could let $\phi = 0$ and a more simplified expression can be given:

$$U_m(R) = \frac{kA_n a_n^2 q}{H_0^2} Jinc\left(\frac{ka_n}{H_0} r_n\right) \exp(jkH_0) \times \sum_{n=1}^{N_m} \exp\left(-jk \frac{Rr_n \cos\alpha}{H_0}\right). \quad (9)$$

We then divided the whole mth ring zone into N_m subzones that include just one circular pinhole each. It is obvious that each subzone subtends a small angle of $\Delta\alpha = 2\pi/N_m$. So, Eq. (9) could be transformed into

$$U_m(R) = \frac{kA_n a_n^2 q}{H_0^2} Jinc\left(\frac{ka_n}{H_0} r_n\right) \exp(jkH_0) \times \frac{N_m}{2\pi} \sum_{n=1}^{N_m} \exp\left(-jk \frac{Rr_n \cos\alpha}{H_0}\right) \Delta\alpha. \quad (10)$$

Note that there are usually hundreds or thousands of holes in each pinhole ring. Then all those $\Delta\alpha$ values are quite small. It is obvious that $\sum_{n=1}^{N_m} \Delta\alpha = 2\pi$ and the function $\exp(-jkRr_n \cos\alpha/H_0)$ is continuous over the interval $[0, 2\pi]$. By replacing the sum sign $\sum$ and $\Delta\alpha$ by the integral sign $\int$ and $d\alpha$, respectively, we can obtain

$$U_m(R) = \frac{kA_n a_n^2 q}{H_0^2} Jinc\left(\frac{ka_n}{H_0} r_n\right) \exp(jkH_0) \times \frac{N_m}{2\pi} \int_0^{2\pi} \exp\left(-jk \frac{Rr_n}{H_0} \cos\alpha\right) d\alpha. \quad (11)$$

Remember that the transformation of Eq. (10) to Eq. (11) is accurate enough only when there is a great number of pinholes in a ring zone. As a specific example, let us check the diffracted field of the 16th pinhole ring of a 0.1 m diameter photon sieve illuminated normally by a plane wave with wavelength $\lambda = 532$ nm. The pinholes in the PS are located in the bright zones, which means $r_n^2 = 2nf\lambda + n^2\lambda^2$ and the width w of each zone is $w = \lambda f/(2r_n)$. The pinhole size is chosen to be $d = 1.5w$, where $d = 2a_n$ is the diameter of the pinhole. The angular interval between the centers of each two circular pinholes is $2d/r_n$, $R = 0.2$ mm and $q = 1$ m, respectively. We can prove that there are 134 pinholes in this ring zone. The calculated complex diffracted fields using Eq. (10) and Eq. (11) are 0.041965-0.183859i and 0.041962-0.183851i, respectively.

Extremely high accuracy is achieved for this replacement of the sum by the integral. We did another numerical test that 100 same size pinholes are settled uniformly in this ring zone. Calculations show that the extremely high accuracy is maintained. Thus we reasonably proposed a general criterion that the number of pinholes in each ring zone N_m should be more than 100. Under such condition, the replacement of the sum by the integral is highly accurate.

Employing the equality in Ref. [10]:

$$J_0(-v) = \frac{1}{2\pi} \int_0^{2\pi} \exp(-jv\cos\alpha) d\alpha, \quad (12)$$

and the property $J_0(-v) = J_0(v)$, where $v = kRr_n/H_0$, one can further get

$$U_m(R) = N_m \frac{kA_n a_n^2 q}{H_0^2} Jinc\left(\frac{ka_n}{H_0} r_n\right) \exp(jkH_0) J_0\left(\frac{kRr_n}{H_0}\right). \quad (13)$$

Equation (13) is the analytical expression for the diffracted field of the individual pinhole ring. In terms of the linear superposition principle, the overall diffracted light field for all of the pinhole rings could be given by

$$U(R) = \sum_{m=m1}^{M} N_m \frac{kA_n a_n^2 q}{H_0^2} Jinc\left(\frac{ka_n}{H_0} r_n\right) \exp(jkH_0) J_0\left(\frac{kRr_n}{H_0}\right), \quad (14)$$

where the value of $m1$ is the minimum ring order for which the sufficient conditions of pinhole ring diffraction model are satisfied. Equation (14) can be used to compute the focusing of a large PS at an extremely fast speed.

3. PS SIMULATION RESULTS AND ANALYSIS

We then analyzed the validity of the pinhole ring diffraction model by investigating the 0.1 m diameter photon sieve mentioned in the last part of Section 2. Table 1 lists the parameters. Figure 2 shows an image of the central 20 pinhole rings of the PS, with rings of order $m = 1\sim20$.

To deduce the analytical expression for the diffracted field of the pinhole ring diffraction model, some approximations have been done during the transform from Eq. (4) to Eq. (8). We found that these approximations are highly valid when the diffracted field region is quite near the focal point ($X = 0$, $Y = 0$). Concretely, we pointed out that $R/r_n \le 0.05$ could be used as general criterion. Then we checked the validity of this criterion. The criterion could be rewritten as

$$r_n \ge 20R_{\text{Max}}. \quad (15)$$

In other words, when the maximum focal region R_{Max} is determined, it is recommended to use the pinhole ring diffraction model for higher order pinhole rings whose radii are bigger than $20R_{\text{Max}}$. Let us investigate the diffracted field within the radius $R_{\text{Max}} = 0.2$ mm, which is good enough to describe the focusing property for 0.1 m diameter PS prototype. So the minimum pinhole ring radius r_n should be bigger than $20R_{\text{Max}} = 4$ mm and the corresponding ring order is 16. The Fresnel number N_f of pinholes in the 16th ring is smaller than 0.05. First the diffracted fields along X axis coordinate on the focal plane for individual pinholes in the 16th ring also

Table 1. Design Parameters of the 0.1 m Diameter Photon Sieve

Photon Sieve Property	Value
Diameter D	0.1 m
Focal Length f	1 m
Wavelength λ	532 nm
d/w factor	1.5
Number of Pinholes	23,092,272
Number of Rings	2348
Hole Size Range	4–193 microns

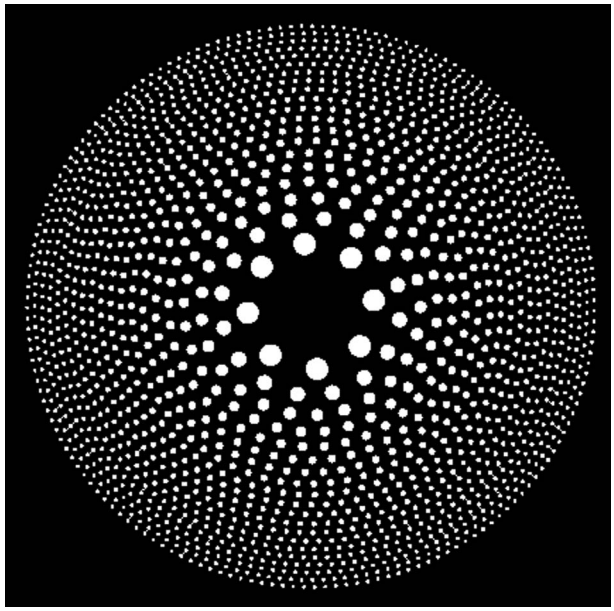

Fig. 2. Central 20 pinhole rings of the photon sieve.

are calculated using Eq. (4). Then the overall diffracted filed is obtained by the summation of those individual diffracted fields. For comparison, the diffracted fields were computed using Eq. (8) in the pinhole ring model. The real part and imaginary part of the calculated complex diffracted fields are plotted in Figs. 3(a) and 3(b). Note the Y-Axis in Fig. 3(a) has a smaller scale so as to show the deviation of the two curves more clearly. From Fig. 3, we found that the differences between the calculated diffracted field distributions are relatively small when $X \leq 0.1$ mm. For those points 0.1 mm $< X \leq 0.2$ mm, there are small differences. These slight differences illustrated the dependence of the accuracy on the R/r_n value. However, combining the real part and imaginary part, the differences of the overall complex diffracted fields are quite small. These results show that the approximations from Eq. (5) to Eq. (7) are accurate enough for the focusing analysis at the focal region $R/r_n \leq 0.05$. Keep in mind that the ring radius r_n would increase for higher order pinhole ring, which means the pinhole rings in the outer ring zones would have even smaller R/r_n value. This, in turn, leads to a much higher computation accuracy. Note that big or high-NA photon sieves are usually composed of hundreds or thousands of pinhole rings. Despite these small differences for the inner ring zones, the overall diffracted field computed using pinhole ring diffraction model would be very accurate for those big photon sieves.

To further verify the accuracy of the pinhole ring diffraction model, the overall diffracted fields of pinholes within ring order $m = 16$–2348 (23,091,274 pinholes) of the 0.1 m diameter PS were calculated. Then the normalized intensity distributions along X axis on the focal plane were computed and plotted in Fig. 4. The solid lines and asterisks plot in Fig. 4 correspond to the results given by individual pinhole mode and pinhole ring diffraction mode.

During the individual pinhole mode calculation the diffracted fields of the 23,091,274 pinholes are calculated using

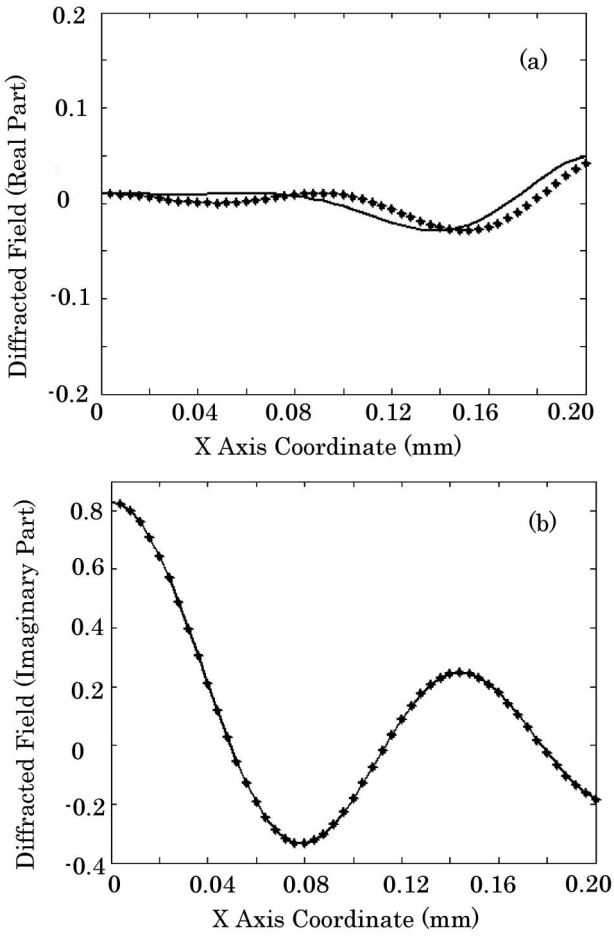

Fig. 3. Comparison of the diffracted fields on the focal plane for the pinholes in the 16th ring zone. The solid lines and the asterisks plot correspond to the diffracted fields computed using Eq. (4) and Eq. (8). (a) The real part of the complex diffracted fields. (b) The imaginary part of the complex diffracted fields.

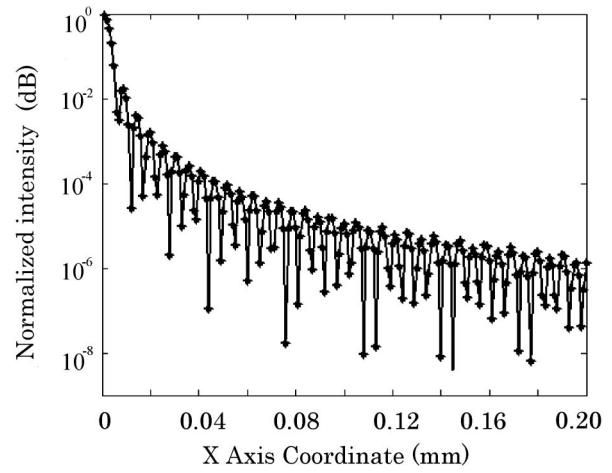

Fig. 4. Comparison of normalized intensity distributions on the focal plane for the pinholes within ring order $m = 16$–2348 of the 0.1 m diameter photon sieve. The solid lines and the asterisks plot correspond to the intensity distributions computed using individual pinhole model and pinhole ring diffraction model.

Eq. (2), respectively, and the results are added up to get the total diffracted fields. The results of pinhole ring diffraction model are calculated as follows: for pinholes within ring order $m = 16–2348$ (23,091,274 pinholes), whose Fresnel numbers $N_f \leq 0.05$ and $r_n \geq 20R_{\mathrm{Max}}$, the diffracted field of the individual pinhole ring are calculated with Eq. (13). And the results of those 2333 rings were added to get the total diffracted fields using Eq. (14).

Figure 4 clearly showed that the differences of the normalized intensity distribution computed by individual pinhole model and pinhole ring diffraction model are quite small across the whole focal region. The RMS value of the differences of the two normalized intensity distributions is 6.59×10^{-9}. Besides, it can be seen that high accuracy has been achieved not only in the main lobe region but also the weak sidelobe region, which were as low as $10^{-6} \sim 10^{-7}$ of the peak intensity. The above calculations are done with a standard desktop computer (a 2.7 GHz processor and 2 GB of memory). The execution times were 5 h, 16 min, and 5 s for the diffracted field calculations using the individual pinhole mode and pinhole ring diffraction mode, respectively. Thus, with pinhole ring diffraction mode, we were able to estimate that the computation time could be less than one minute for the fields of large or high-NA PS. The above discussions have validated the pinhole ring diffraction model for the fast, accurate analysis of a large PS.

4. CONCLUSION

Based on the nonparaxial far-field model of individual pinhole, we have presented a pinhole ring diffraction model for the focusing of large photon sieve. The Fresnel number N_f of those circular pinholes should be smaller than 0.05. The pinholes in each ring zone must have the same size and be distributed uniformly in angle in the ring zone. In addition, the number of pinholes in each ring zone N_m should be more than 100. It also is worth mentioning $R/r_n \leq 0.05$, which means that the analyses in this paper were focused on the diffracted field of the small focal region. The above four prerequisites are the sufficient conditions for the validity of this pinhole ring diffraction model. In such case, all of the pinholes in a ring zone could be treated as a single unit when investigating the diffracted field. An explicit equation within the framework of scalar field has been given to describe the diffracted field of individual pinhole ring. Then the computation of the diffracted fields for millions or billions of pinholes could be reduced to the simplified computation of several hundreds or thousands of pinhole rings.

As a consequence, those pinhole ring diffraction model equations could be used to accurately compute the focusing of large photon sieve at an extremely fast speed. The diffracted field for the pinholes within ring order $m = 16–2348$ of one 0.1 m diameter photon sieve has been calculated using both the individual pinhole model and pinhole ring diffraction model. The investigations and comparison proved that the theory is robust and reliable.

REFERENCES

1. L. Kipp, M. Skibowski, R. L. Johnson, R. Berndt, R. Adelung, S. Harm, and R. Seemann, "Sharper images by focusing soft x-rays with photon sieve," Nature **414**, 184–188 (2001).
2. Q. Cao and J. Jahns, "Focusing analysis of the pinhole photon sieve: photon sieve individual far field model," J. Opt. Soc. Am. A **19**, 2387–2393 (2002).
3. Q. Cao and J. Jahns, "Nonparaxial model for the focusing of high-numerical-aperture photon sieves," J. Opt. Soc. Am. A **20**, 1005–1012 (2003).
4. F. Giménez, J. A. Monsoriu, W. D. Furlan, and A. Pons, "Fractal photon sieve," Opt. Express **14**, 11958–11963 (2006).
5. G. Andersen, "Large optical photon sieve," Opt. Lett. **30**, 2976–2978 (2005).
6. G. Cheng, C. Hu, P. Xu, and T. Xing, "Zernike apodized photon sieves for high-resolution phase-contrast x-ray microscopy," Opt. Lett. **35**, 3610–3612(2010).
7. H.-H. Chung, N. M. Bradman, M. R. Davidson, and P. H. Holloway, "Dual wavelength photon sieves," Opt. Eng. **47**, 118001 (2008).
8. G. Anderson and D. Tullson, "Broadband antihole photon sieve telescope," Appl. Opt. **46**, 3706–3708 (2007).
9. G. Andersen, "Membrane photon sieve telescopes," Proc. SPIE **7731**, 773123 (2010).
10. M. Abramowitz and I. A. Stegun, eds., *Handbook of Mathematical Functions with Formulas, Graphs, and Mathematical Tables* (Wiley, 1972).